Determination of the Symmetric Short-Circuit Currents of Synchronous Permanent Magnet Machines Using Magnetostatic Flux Maps

Determination of the Symmetric Short-Circuit Currents of Synchronous Permanent Magnet Machines Using Magnetostatic Flux Maps

Simone Ferrari, Paolo Ragazzo, Gaetano Dilevrano and Gianmario Pellegrino
Energy Department "Galileo Ferraris"
Politecnico di Torino
Turin, Italy
simone.ferrari@polito.it, paolo.ragazzo@polito.it, gaetano.dilevrano@polito.it gianmario.pellegrino@polito.it

***Abstract*—The three-phase symmetric short-circuit is a reference fault condition for the qualification of a newly designed permanent magnet (PM) synchronous machine against the risk of irreversible demagnetization. To date, the accurate determination of the peak transient short-circuit current condition requires coupled circuital and transient Finite Element Analysis (FEA) to take magnetic saturation properly into account, and several simulations to determine the worst case pre-fault conditions. This work presents a method for the fast evaluation of the transient short-circuit currents of a PM synchronous machine by manipulation of its flux linkage maps, using the maps obtained via magnetostatic FEA. Besides providing a fast and accessible means of estimate, the flux-map based method gives insights on the effect of the pre-fault conditions, showing that the higher the initial flux linkage, the worse, and that generator operation is more severe than motor operation. The hyper-worst-case short circuit concept is also defined, which is a magnetic property of the machine under test, and a procedure for its fast-FEA computation is given. The method is validated against the results of transient FEA obtained using a commercial software.**

I. Introduction

The symmetric three-phase short-circuit is a reference fault condition for Permanent Magnet (PM) synchronous machines, to be carefully considered to avoid the risk of irreversible demagnetization [1]–[3]. While the steady-state fault current is easily calculated as the machine characteristic current i_{ch}, the estimation of the peak transient short-circuit current requires a transient simulation [4]. Saturation of the q axis is considered in [5], but the cross-saturation effects are neglected. A full analytical model to predict the symmetric short circuit was proposed in [6], without any support from FEA simulations and thus neglecting the cross-saturation effect. In [7] the saturation of both axes is contemplated using FEA results in a number of operating points, which is in the direction of what proposed here. To date, the use of transient FEA coupled to circuital simulation is retained the most accurate solution, although being time consuming [8] and restricted to commercial software tools only. Last, other types of short-circuit have been analysed in literature: [9] [10] studied the prediction of the partial-turn short-circuit, single-phase open circuit fault and phase-to-phase terminal short-circuit.

The paper introduces a method for the fast and accurate determination of the peak short-circuit current under symmetric fault conditions, computed by off-line manipulation of the motor flux maps. The results are validated against dynamic simulations in Matlab/Simulink [11] and transient FEA computation coupled with circuital model using Simcenter MAGNET [12].

The analysis of pre-fault conditions and response of different interior PM synchronous machines is also developed and discussed. Conclusions are derived from both analyses. Finally, a fast FEA method to estimate the peak short-circuit current without pre-evaluated flux maps will be introduced, and the hyper-worst-case (hwc) short-circuit current is defined. The proposed methods are viable for all synchronous machines described through flux maps, including Surface-mounted PM (SPM) machines, Interior PM (IPM) machines, PM-assisted Synchronous Reluctance (PM-SyR) machines and even Synchronous Reluctance (SyR), although this is of little interest. Magneto-static FEA is retained fully accurate for interior PM machines (IPM and PM-SyR) and also accurate for SPM machines with segmented magnets, where the eddy-currents are not intense enough to modify the magneto-static field distribution.

The transient short-circuit current evaluation functionality is

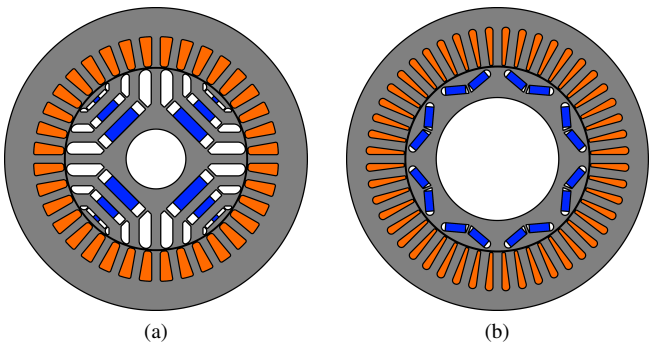

(a) (b)

Fig. 1: Cross section of the THOR and PRIUS machine examples used in the paper, with the PMs colored in blue.

TABLE I: Ratings of the motors under test

		THOR	PRIUS	
Number of pole pairs	p	2	4	
Max current	i_{max}	44	250	[Apk]
Characteristic current	i_{ch}	1	0.34	[p.u.]
DC link voltage	V_{dc}	310	650	[V]
Max torque	T_{max}	43	200	[Nm]
Nominal speed	n_{nom}	2500	3000	[rpm]
Max speed	n_{max}	9000	12000	[rpm]
Max power	P_{max}	11.5	60	[kW]

included into the open-source design environment SyR-e [13]. The results presented in the paper refer to a PM-SyR machine for light traction named THOR [14] and to the primary electric motor of the 2010 Toyota Prius Hybrid Synergy Drive [15], an IPM machine here indicated as PRIUS. The cross sections of the two considered motors are shown in Fig. 1, and the ratings are in Table I.

II. Short-Circuit Model based on Flux Maps

The voltage equations of the synchronous machine are reported in (1).

$$\begin{cases} v_d = R_s \cdot i_d - \omega \cdot \lambda_q + \frac{d\lambda_d}{dt} \\ v_q = R_s \cdot i_q + \omega \cdot \lambda_d + \frac{d\lambda_q}{dt} \end{cases} \tag{1}$$

where v_d and v_q are the dq voltages of the motor, i_d and i_q the dq currents, λ_d and λ_q the dq flux linkages, R_s the phase resistance and ω the electric pulsation in rad/s, related to the rotor speed in revolutions per minute $n = \frac{\omega}{p} \cdot \frac{30}{\pi}$ by way of the number of pole pairs p. For the sake of generality, the flux linkages are defined in the form of flux maps (2):

$$\begin{cases} \lambda_d = \mathbf{\Lambda}_d(i_d, i_q) \\ \lambda_q = \mathbf{\Lambda}_q(i_d, i_q) \end{cases} \tag{2}$$

All maps function of (i_d, i_q) will be denoted with bold capital letters. The electromagnetic torque equation is:

$$T = \tfrac{3}{2} p \cdot (\lambda_d \cdot i_q - \lambda_q \cdot i_d) \tag{3}$$

and the corresponding map can be obtained by substituting the current and flux maps into the equation:

$$\mathbf{T} = \tfrac{3}{2} p \cdot (\mathbf{\Lambda}_d \odot \mathbf{I}_q - \mathbf{\Lambda}_q \odot \mathbf{I}_d) \tag{4}$$

where $\mathbf{I}_d, \mathbf{I}_q$ is the mesh defining the i_d, i_q domain and the symbol $\odot$ indicates the matrix element-wise product.

A. Steady-State Short-Circuit Solution

The steady-state voltage maps $\mathbf{V}_d(i_d, i_q)$, $\mathbf{V}_q(i_d, i_q)$ (5) are computed by substituting the flux and current maps in the steady-state form of (1).

$$\begin{cases} \mathbf{V}_d = R_s \cdot \mathbf{I}_d - \omega \cdot \mathbf{\Lambda}_q \\ \mathbf{V}_q = R_s \cdot \mathbf{I}_q + \omega \cdot \mathbf{\Lambda}_q \end{cases} \tag{5}$$

For each considered angular frequency ω, the steady-state short circuit current is found by imposing both voltage components to zero. Using the voltage maps, the $v_d = 0, v_q = 0$ contours are found, their intersection point i_{ss} being the steady-state short-circuit current. This is graphically described in Fig. 2 for the THOR machine at nominal speed. Please notice that the SyR machines convention for the dq axes, i.e. the PM flux linkage is q-negative. Accordingly, the short circuit current aligns against the PM direction, and being the speed high enough it coincides with the characteristic current $i_{ch} = 43$ A, at the considered temperature of 20°C.

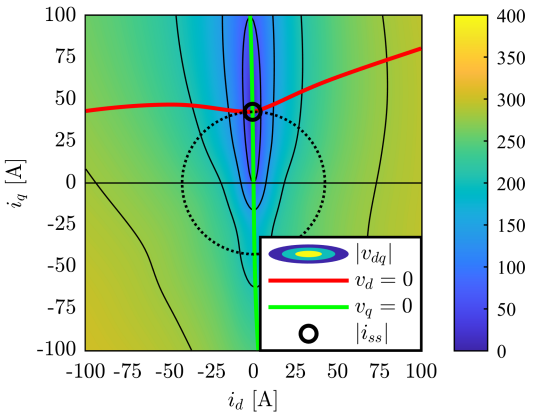

Fig. 2: Computation of i_{ss} (black circle) at 2500 rpm.

The steady-state flux and torque in short-circuit conditions are found by interpolating the respective maps at $(i_{d,ss}, i_{q,ss})$. The process is repeated for a number of angular frequencies to trace the short-circuit current, flux-linkage and torque versus speed characteristics, reported in Fig. 3. The torque is negative (i.e. braking) at all speeds with a peak of 16 Nm (37% p.u.) at 125 rpm and it tends asymptotically to zero for higher speed values. Looking at the current characteristics, as the torque tends to zero, the current vector tends to align asymptotically to the q axis, i.e. to the characteristic current condition. The asymptote corresponds to zero flux linkage, as evidenced by the flux characteristic.

B. Transient Short-Circuit Computation

The transient short-circuit current waveforms are calculated solving the voltage equation in discrete-time form. For the sake of simplification, iron losses are neglected and the rotor speed is considered constant. Both assumptions are conservative, as demonstrated in the following sections.

The voltage equation (1) is turned into discrete-time form using the Euler method (6). Δt is the time step and the superscripts k and $k+1$ indicate the present and next time samples, respectively, at $t = t_k$ and $t = t_k + \Delta t$.

$$\begin{cases} \lambda_d^{k+1} = \lambda_d^k + \left(-R_s \cdot i_d^k + \omega \cdot \lambda_q^k\right) \cdot \Delta t \\ \lambda_q^{k+1} = \lambda_q^k + \left(-R_s \cdot i_q^k - \omega \cdot \lambda_d^k\right) \cdot \Delta t \end{cases} \tag{6}$$

The currents at $k+1$ are calculated using the inverse flux maps:

$$\begin{cases} i_d^{k+1} = \mathbf{I}_d(\lambda_d^{k+1}, \lambda_q^{k+1}) \\ i_q^{k+1} = \mathbf{I}_q(\lambda_d^{k+1}, \lambda_q^{k+1}) \end{cases} \tag{7}$$

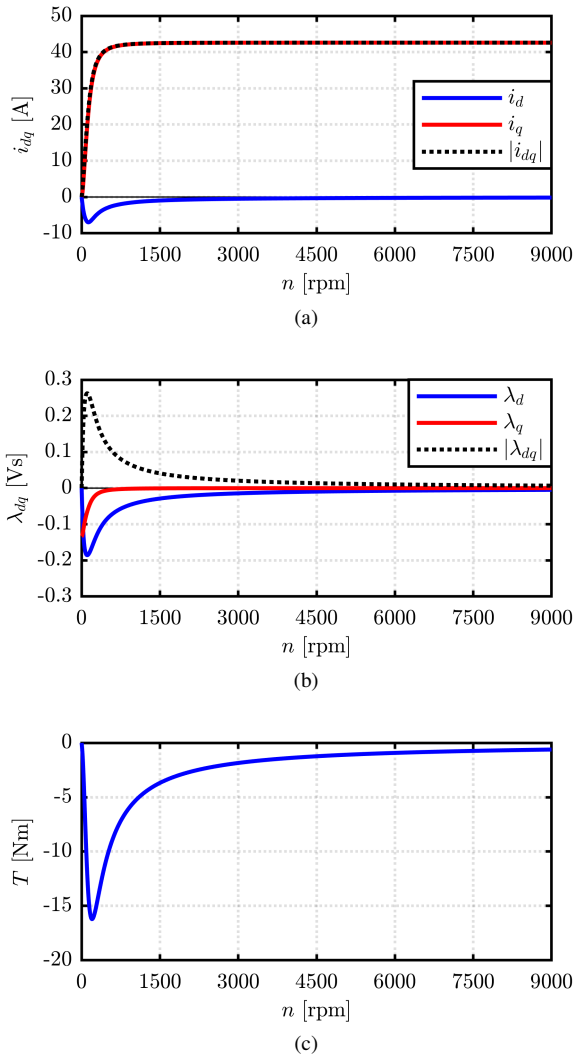

Fig. 3: Steady-state short-circuit (a) currents, (b) flux linkages and (c) torque of the THOR machine, function of rotor speed.

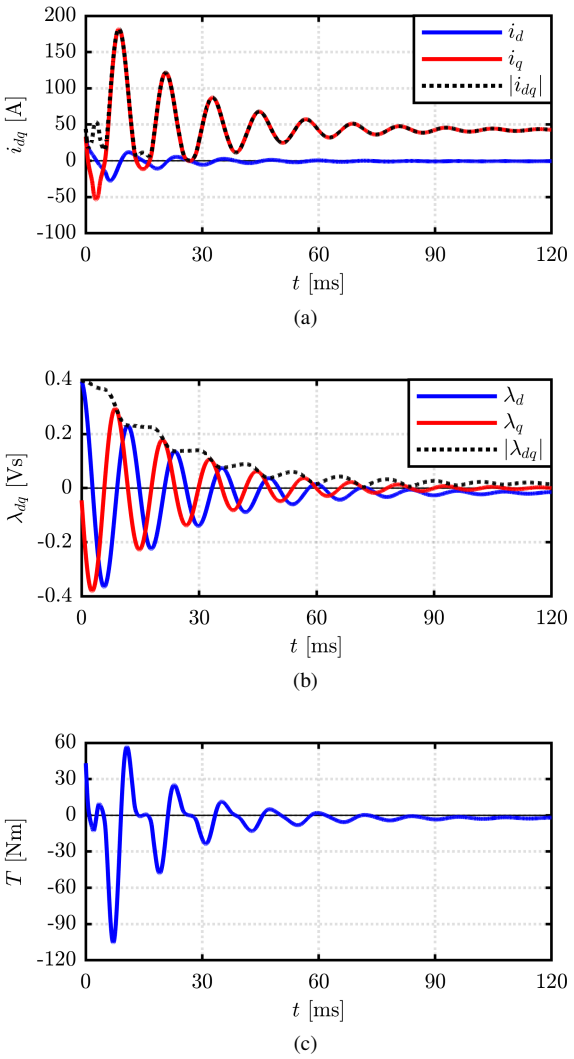

Fig. 4: Results of the short circuit computation for the THOR machine: (a) dq currents, (b) dq flux linkages, (c) torque function of time.

The inverse flux-maps $\mathbf{I}_d(\lambda_d, \lambda_q)$, $\mathbf{I}_q(\lambda_d, \lambda_q)$, or the maps of current function of flux linkage components, are obtained by manipulation of the current-input flux maps, as described in [16]. Finally, the electromagnetic torque is found from the torque map:

$$T^{k+1} = \mathbf{T}(i_d^{k+1}, i_q^{k+1}) \tag{8}$$

The resulting waveforms are displayed in Fig. 4 for a time window of ten cycles. The worst-case pre-fault conditions are considered, which is at the maximum current amplitude and maximum torque per ampere (MTPA) conditions, as will be clarified later. The peak short circuit current occurs after half cycle circa and has a value of 183 A (4.25 times the steady-state fault current). The peak torque occurs in the neighborhoods of the current peak and is worth 105 Nm, i.e. 2.44 times the maximum torque of the THOR machine. The initial flux amplitude has a key role in the determination of the peak current, as will be explained later. The waveforms steady-state conditions coincide with what predicted by the steady-state analysis. The computational time needed to calculate ten electrical cycles is about 16 seconds, whereas covering one period to spot the peak transient current takes about 1.5 seconds. The computer in use is a laptop with an Intel i7-8750H CPU and 16 GB of RAM.

C. Current and Flux Trajectories

The current and flux linkage trajectories during the symmetric short circuit are shown in Fig. 5, represented by the red lines of sub-figures (a) and (b) respectively. The initial point or pre-fault condition is indicated with a red circle, and the steady-state solution is the green cross. The flux linkage follows a spiral trajectory starting from the pre-fault MTPA condition which is also the maximum flux condition for this machine. The rate of decay of the flux amplitude relates to the combination of stator resistance loss and rotor speed,

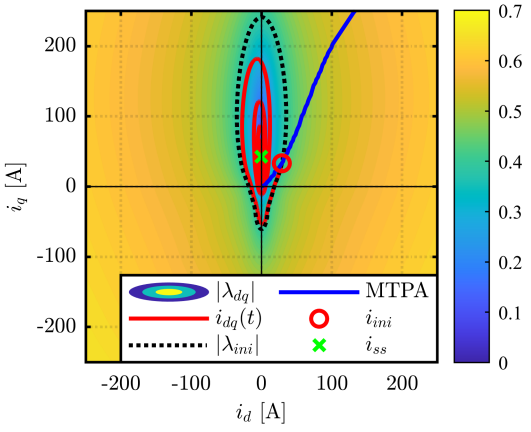

(a)

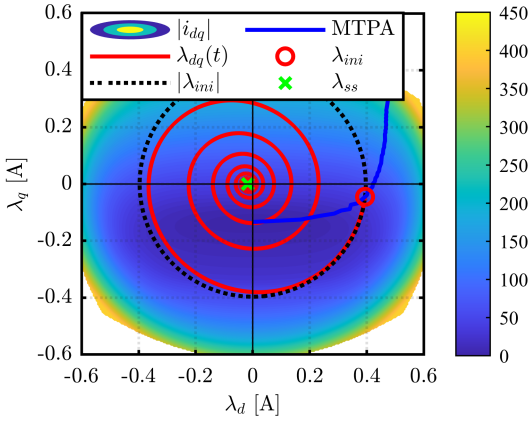

(b)

Fig. 5: (a) Current and (b) flux linkage trajectories during the short-circuit on the respective dq planes.

considering that no other type of loss is accounted for in this model. With no loss, the flux linkage vector would move clock-wise on a circle. The dq current trajectory corresponding to the spiral flux trajectory is reported along with the dashed black line corresponding to the maximum flux locus in the current plane. Seen the clock-wise rotation, a first current peak is found along the negative q axis and the maximum current condition is then found along the positive q axis, half cycle later. The distance between the maximum current value (183 A) and the maximum of the constant-flux dashed trajectory (240 A) relates to the decay of the flux spiral, i.e. to the damping effect of stator Joule loss. The higher the loss, the faster the decay, the lower the peak current. This justifies the assumption that neglecting the iron loss or other loss terms in the model is on the safe side. The maximum of the dashed trajectory is defined as hyper-worst-case (HWC) short-circuit current $i_{pk,hwc}$.

D. Fast FEA Estimation of the Hyper-Worst-Case Current

The flux and current trajectories of Fig. 5 suggest a method to estimate the HWC short circuit current by few FEA simulations, without flux maps. The $i_{pk,hwc}$ is found by searching the current aligned against the PMs that corresponds to the pre-fault flux linkage amplitude. This is found iteratively using the secant method. Assuming that the pre-fault condition λ_{max} (maximum torque at MTPA) is known, the linear equation (9) must be solved function of i_q and being the function $\lambda_q(0, i_q)$ unknown.

$$f(i_q) = \lambda_q(0, i_q) - \lambda_{max} = 0 \tag{9}$$

The examples of Fig. 6 refers to THOR machine and use the SyR-style axes. Using the PM-style axes, the equation to be solved function of i_d would be $f(i_d) = \lambda_d(0, i_d) + \lambda_{max} = 0$. Fig. 6 reports the $\lambda_q(0, i_q)$ function with black solid line for reference and with colored circles the FEA-simulated points during the iterative solution. The solution of (9) can be represented graphically as the intersection between the $\lambda_q(0, i_q)$ curve (solid black line) and the λ_{max} line (horizontal black line of Fig. 6). The iterative process is explicitly shown in Fig. 6 just for the first iteration for a sake of clarity. The first two FEA simulations are the blue and red point, close to the maximum current. The next FEA point is obtained as the interception between the line through the last two FEA-simulated point (reported in dashed black line) and the λ_{max} line (horizontal black line). The intersection is reported with green triangle, and the FEA result with green circle. The iterative process continue until the FEA result is equal to λ_{max} (with a tolerance of 10%, to ease the process convergence). The final result is reported in turquoise circle, and the $i_{pk,hwc}$ is marked with a vertical black line.

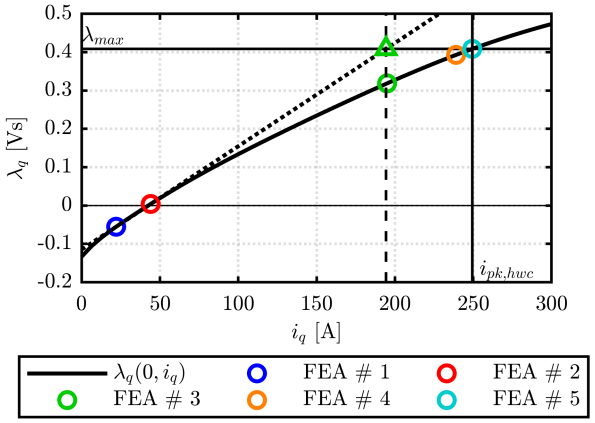

Fig. 6: Identification of the HWC peak current: PM axis reported in solid black line and FEA simulated points during iterations reported with colored circle.

The strength of this process is the fact that, with the simple FEA model and without flux maps or equivalent circuit parameters, it is possible to have a pessimistic estimation of the peak current during short-circuit in few minutes, allowing

a rapid check on the PM demagnetization in the very first step of the machine design.

III. Validation of the Proposed Model

A. Validation Against Simulink

The proposed procedure is validated against the Simulink model of the machine, based on the same inverse flux maps, used in (7). The Simulink model takes into account the finite rotor inertia and the rotational loss terms of friction, viscosity and ventilation, and the iron loss term. It is assumed that before the short circuit the motor runs at constant speed at maximum torque. When the short circuit occurs the speed decreases due to the combined effects of mechanical and electrical losses (copper and iron). The worst case condition of maximum torque 43 Nm at nominal speed 2500 rpm is analysed. The comparative results of Fig. 7 show that the two solutions are pretty well superimposed, with the exception of the effect of speed change which relents the oscillation frequency over time and reduces the torque and current peak values. This confirms the affirmation of the constant-speed assumption being a conservative condition.

B. Validation Against Transient FEA

A further validation is given against transient FEA performed in Simcenter MAGNET [12]. The simulation is coupled with circuit analysis reported in Fig. 9: the three-phase windings are star connected and each phase is supplied by a current generator, according to the willed pre-fault conditions. The fault is provoked by two automatic switches ($S10 - S11$ in Fig. 9) that deviate the current generators output and short-circuit the machine terminals. The calculation in MAGNET, with step of 0.1 ms and a simulation time of 120 ms takes about 20 minutes on the same laptop PC.

With reference to the worst case initial condition of MTPA and maximum torque at nominal speed, overload current at base speed the current and torque waveforms overlap very well Fig. 8, including the peak values. The enhanced time window of Fig. 8 shows harmonic components not accounted for in the fundamental flux map model.

C. Effect of the Pre-Fault Conditions

As suggested from the analysis of the dq current and flux trajectories the pre-fault condition has a huge impact on the peak short circuit current. In the following, three pre-fault conditions will be compared.

1) no load at 2500 rpm;
2) T_{max} at 2500 rpm;
3) $-T_{max}$ at 2500 rpm.

The same speed is used in all the examples for ease of comparison. Fig. 10 shows the current waveform function of the time for the considered pre-fault conditions. In the plot, the circle and asterisks denote respectively the initial and peak current points in time. This points are also reported in Table II for a quick comparison.

The results evidence that the no-load condition is the least severe because the initial flux linkage amplitude is the lowest, according to their current trajectory amplitude. This is clarified by the (i_d, i_q) and (λ_d, λ_q) fault trajectories reported in Fig. 11. Dealing with the maximum torque scenarios, the motoring case is slightly less critical than braking even if the initial flux amplitude is purposely the same. Given that the flux spiral is traveled clock-wise, having the initial point in the first quadrant (motor) or second quadrant (brake) means a longer or shorter time to reach the maximum current condition, and thus a longer or shorter decay time. In turn, when braking the peak short circuit current happens within half a cycle, whereas

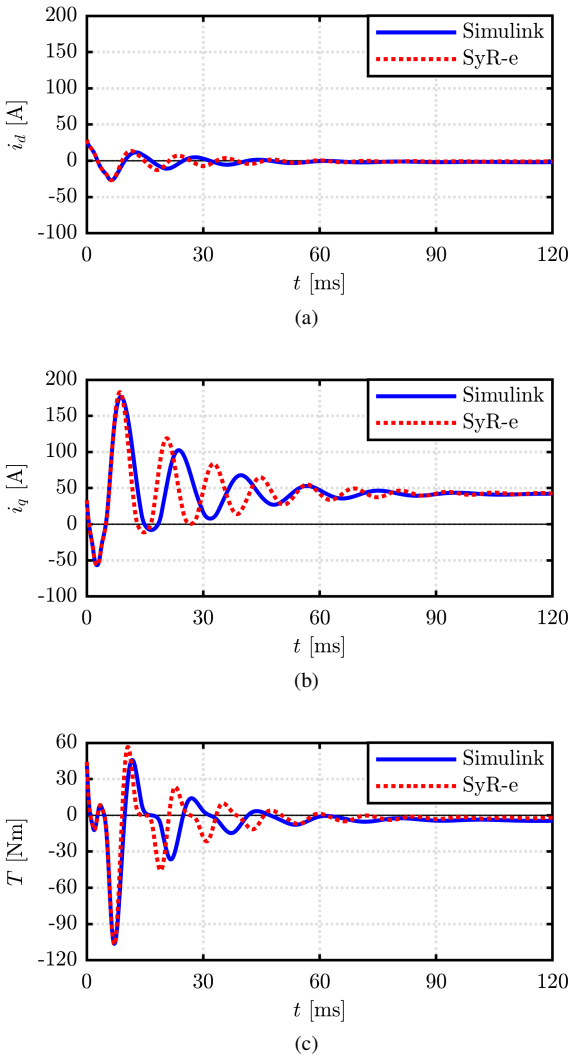

Fig. 7: Results of the short circuit computation with the proposed method at constant speed (red dotted line) and Simulink model at variable speed (solid blue line): (a) d-axis current, (b) q-axis current and (c) torque.

TABLE II: Comparison between different pre-fault conditions

Scenario	$\lvert i_{max}\rvert$ [A]	$\lvert i_{pk}\rvert$ [A]	$\lvert\lambda_{max}\rvert$ [mVs]	$\lvert\lambda\rvert@i_{pk}$ [mVs]
no load	0	85.8	134	109
T_{max}	44	182.1	397	306
$-T_{max}$	44	195.5	397	331

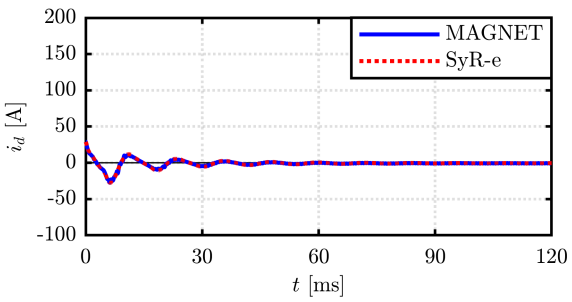

(a)

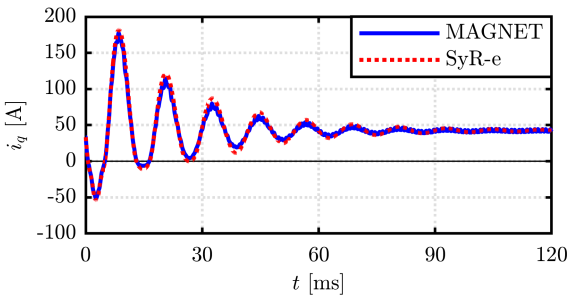

(b)

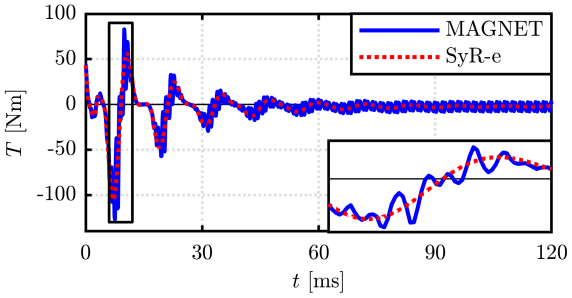

(c)

Fig. 8: Results of the short circuit computation with the proposed method and transient simulation: (a) d-axis current, (b) q-axis current and (c) torque function of time with pre-fault condition equal to 43 Nm along the MTPA.

when motoring it happens at the second half cycle.

D. Effect of the Speed

The rotor speed has effect on both the steady-state and peak current and torque values. The same initial condition of peak torque at MTPA is studied here at three different speeds:

- $n = 125$ rpm, corresponding to the maximum value of steady-state short circuit current;
- $n = 2500$ rpm, that is the base speed;
- $n = 9000$ rpm, that is the maximum speed. This is not a feasible point because of the voltage limit, but is considered as extreme point for a sake of comparison.

The results of the three simulations are reported in Fig. 12. Current, flux linkage and torque are the terms of comparison, on the same time scale (one period at 125 rpm, meaning 240 ms). At low speed there is no overcurrent and the braking

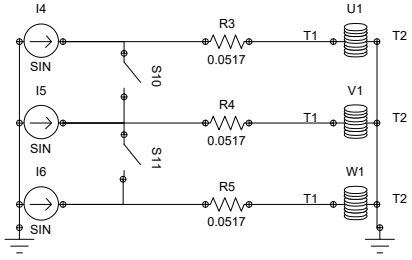

Fig. 9: Circuit built in MAGNET to simulate the short-circuit.

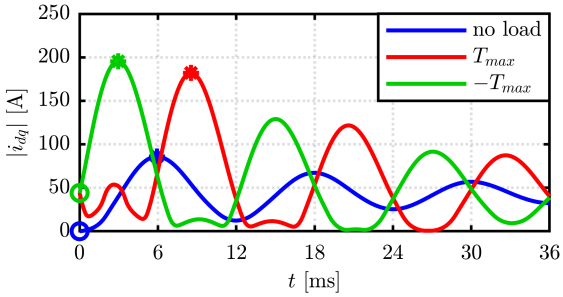

Fig. 10: Comparison of current waveform during the initial cycles of the fault for the considered pre-fault conditions. Maximum current conditions are marked with asterisks.

torque converge to a significant steady-state value. For the other two scenarios the different frequency oscillation results in different peak overcurrent and braking torque values. As the flux amplitude decay is the same in the two cases, the higher the frequency the earlier the peak alignment condition is found, and thus the higher is the peak short-circuit current.

E. Comparison of Different Motors

The effect of the rotor geometry and of the PM quantity are analysed by comparing the results of the two different machines displayed in Fig. 1 with the ratings of Table I.

The short-circuit analysis is executed for both motors at their base speed and at their maximum torque as pre-fault condition. The results are reported in Fig. 13 and Table III, in per-unit of the pre-fault current amplitude of each motor, for ease of comparison. As said, the PM flux linkage of the THOR machine is in the negative q direction, while the PRIUS has the d axis aligned with the PMs. This explains the different orientation of the current trajectories in the dq plane.

The shape of the constant flux linkage contour of the two machines is very much different. Notably, an increased rotor saliency makes such contours sharper, as it is the case of the THOR motor, with the effect of a higher ratio between the transient and the steady-state short circuit current.

As reported in Table I, the THOR motor is designed with a characteristic current equal to its maximum current, whilst the PRIUS characteristic current is roughly equal to one third of its maximum current. Since the steady-state current can be approximated with the characteristic current, the parameter i_{ss}/i_{max} can be easily forecast from motor ratings. However,

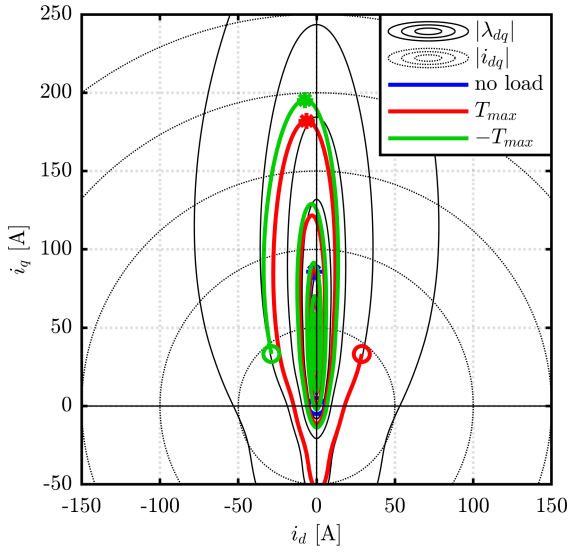

(a)

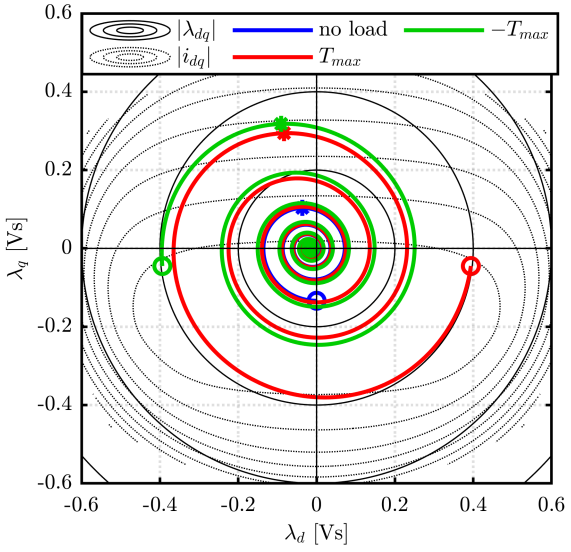

(b)

Fig. 11: Short-circuit trajectories on (a) the (i_d, i_q) and (b) (λ_d, λ_q) plane for the three considered pre-fault scenarios.

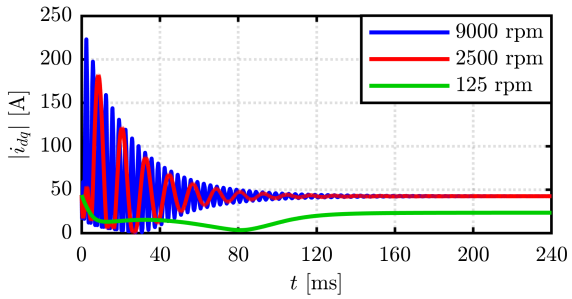

(a)

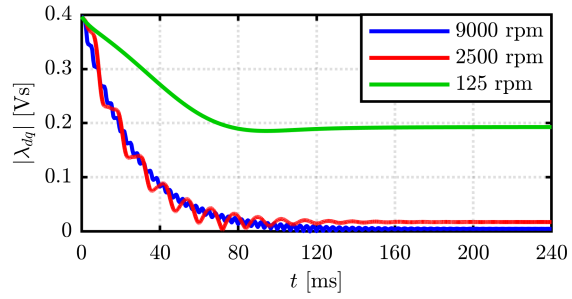

(b)

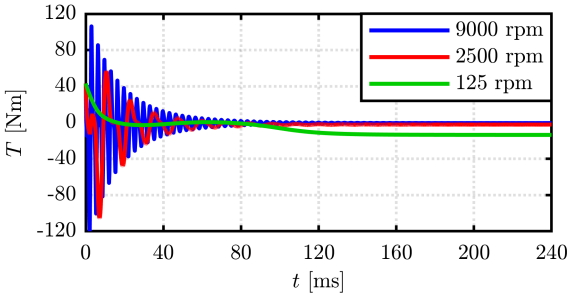

(c)

Fig. 12: Comparison of (a) current and (b) flux linkage waveform for the three considered rotor speed.

TABLE III: Comparison of Short-Circuit for different Motors

	THOR	PRIUS
i_{ss}/i_{max}	1.00	0.35
$i_{pk,hwc}/i_{ss}$	5.7	5.5
i_{pk}/i_{ss}	4.21	4.33
T_{pk}/T_{max}	2.44	1.00

this design choices does not affect the short-circuit severity, as pointed out from the parameters $i_{pk,hwc}/i_{ss}$ and i_{pk}/i_{ss}, that have similar values for the two motors. The former represent the HWC estimation and is around 5.6 for both motors, with a small penalization of THOR, because of the higher saliency. The latter ratio gives a more precise estimation of the peak current during short circuit, around 4 times the steady-state short circuit current for both motors. These values are important for the demagnetization check of PM motors.

The last comparison of Table III deals with the peak braking torque during the short-circuit. This is more severe for the THOR since it reaches about 2.4 times the maximum torque, while the PRIUS peak braking torque is equal to its maximum torque, hence it is less harsh. This data are significant for the mechanical sizing of the shaft connection of the motor to its load.

IV. Conclusions

The proposed paper presents a fast and insightful method for the calculation of the symmetric short-circuit current and torque of PM synchronous machines, based on the integration of the machine voltage equations and the use of FEA flux

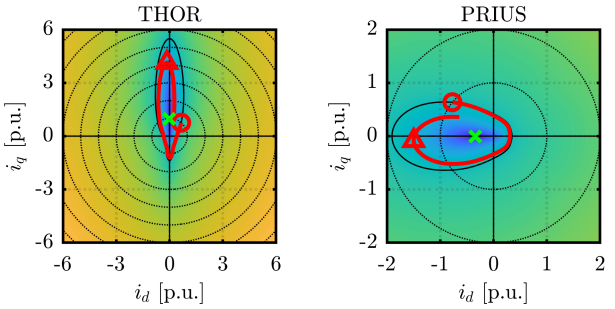

Fig. 13: First cycle of the short-circuit transient for (a) THOR and (b) PRIUS motors. The constant-flux linkage contour is the black line, the red line is the i_d, i_q trajectory, the green cross is the steady-state condition.

maps. The use of flux maps permits the accurate evaluation of the short-circuit transient in reasonable time. The computation is validated against a circuit-coupled dedicated transient FEA in Simcenter MAGNET, showing excellent accuracy. Another method is proposed, for the fast FEA evaluation of the peak current value, without pre-calculated flux maps. The hyper-worst-case current peak is defined accordingly.

The flux-maps based analysis gives insights on the effects of the machine characteristics and the pre-fault conditions with respect to the short-circuit transient. The paper shows that the higher is the pre-fault load (i.e. flux amplitude), the worse is the short-circuit current, and that braking mode is a more severe initial condition. Also, it was demonstrated that any type of loss helps mitigating the peak current. Furthermore, the effect of speed is also addresses, at steady-state and transient conditions.

Dealing with the motor characteristics, two motors with different share of PM and reluctance torque were compared. The parameter $i_{pk,hwc}/i_{pk,ss}$ summarizes the severity of the transient peak current with reference to the steady-state current, and reflects the saliency of the considered machine.

As said, all the procedures presented in the paper are also included in the open-source project SyR-e, to the benefit of academic and industrial community.

Acknowledgment

The research has been conducted with the support of Power Electronics Innovation Center (PEIC) of Politecnico di Torino.

References

[1] S. Ruoho, J. Kolehmainen, J. Ikaheimo, and A. Arkkio, "Interdependence of Demagnetization, Loading, and Temperature Rise in a Permanent-Magnet Synchronous Motor," *IEEE Transactions on Magnetics*, vol. 46, no. 3, pp. 949–953, Mar. 2010.

[2] K.-C. Kim, S.-B. Lim, D.-H. Koo, and J. Lee, "The Shape Design of Permanent Magnet for Permanent Magnet Synchronous Motor Considering Partial Demagnetization," *IEEE Transactions on Magnetics*, vol. 42, no. 10, pp. 3485–3487, Oct. 2006.

[3] J. Hong, S. Park, D. Hyun, T.-j. Kang, S. B. Lee, C. Kral, and A. Haumer, "Detection and Classification of Rotor Demagnetization and Eccentricity Faults for PM Synchronous Motors," *IEEE Transactions on Industry Applications*, vol. 48, no. 3, pp. 923–932, May 2012.

[4] M. Meyer and J. Bocker, "Transient peak currents in permanent magnet synchronous motors for symmetrical short circuits," in *International Symposium on Power Electronics, Electrical Drives, Automation and Motion. SPEEDAM.* Taormina, Italy: IEEE, 2006, pp. 404–409.

[5] B. A. Welchko, T. M. Jahns, W. L. Soong, and J. M. Nagashima, "IPM synchronous machine drive response to symmetrical and asymmetrical short circuit faults," *IEEE Transactions on Energy Conversion*, vol. 18, no. 2, pp. 291–298, Jun. 2003.

[6] W. Q. Chu and Z. Q. Zhu, "Analytical modeling and investigation of transient response of PM machines with 3-phase short-circuit fault," in *2011 IEEE International Electric Machines Drives Conference (IEMDC)*, May 2011, pp. 125–130.

[7] J. D. McFarland and T. M. Jahns, "Investigation of the Rotor Demagnetization Characteristics of Interior PM Synchronous Machines During Fault Conditions," *IEEE Transactions on Industry Applications*, vol. 50, no. 4, pp. 2768–2775, Jul. 2014.

[8] J. Faiz and E. Mazaheri-Tehrani, "Demagnetization Modeling and Fault Diagnosing Techniques in Permanent Magnet Machines Under Stationary and Nonstationary Conditions: An Overview," *IEEE Transactions on Industry Applications*, vol. 53, no. 3, pp. 2772–2785, May 2017.

[9] Z. Sun, J. Wang, D. Howe, and G. Jewell, "Analytical Prediction of the Short-Circuit Current in Fault-Tolerant Permanent-Magnet Machines," *IEEE Transactions on Industrial Electronics*, vol. 55, no. 12, pp. 4210–4217, Dec. 2008.

[10] Min Dai, A. Keyhani, and T. Sebastian, "Fault analysis of a PM brushless DC Motor using finite element method," *IEEE Transactions on Energy Conversion*, vol. 20, no. 1, pp. 1–6, Mar. 2005.

[11] MathWorks, "Simulink." [Online]. Available: https://www.mathworks.com/products/simulink.html

[12] Siemens, "Simcenter MagNet." [Online]. Available: plm.automation.siemens.com/global/en/products/simcenter/magnet.html

[13] F. Cupertino and G. Pellegrino, "SyR-e: Synchronous Reluctance (machines) - evolution." [Online]. Available: www.github.com/SyR-e

[14] S. Ferrari, E. Armando, and G. Pellegrino, "Torque Ripple Minimization of PM-assisted Synchronous Reluctance Machines via Asymmetric Rotor Poles," in *2019 IEEE Energy Conversion Congress and Exposition (ECCE)*, Sep. 2019, pp. 4895–4902, iSSN: 2329-3748.

[15] B. Ozpineci, "Oak Ridge National Laboratory Annual Progress Report for the Electric Drive Technologies Program," Oak Ridge National Lab. (ORNL), Oak Ridge, TN (United States). Power Electronics and Electric Machinery Research Facility, Tech. Rep. ORNL/SPR-2015/626, Oct. 2015. [Online]. Available: https://www.osti.gov/biblio/1235840

[16] S. Ferrari, G. Dilevrano, P. Ragazzo, and G. Pellegrino, "The dq-theta Flux Map Model of Synchronous Machines," in *2021 IEEE Energy Conversion Congress and Exposition (ECCE)*, Oct. 2021.